Chemical Engineering Science 282 (2023) 119346

Contents lists available at ScienceDirect

Chemical Engineering Science

journal homepage: www.elsevier.com/locate/ces

Revisiting the stability of aluminum current collectors in carbonate electrolytes for High-Voltage Li-ion batteries

Leif Nyholm [a,*], Tove Ericson [a], Ahmed S. Etman [a,b,*]

[a] Department of Chemistry–Ångström Laboratory, Uppsala University, SE-75121 Uppsala, Sweden
[b] Department of Chemistry, Faculty of Science, Alexandria University, Ibrahimia, Alexandria 21321, Egypt

A B S T R A C T

Anodic dissolution (often referred to as corrosion) of the aluminum positive electrode current collector above 3 V vs. Li^+/Li can become performance-limiting in high-voltage Li-ion batteries. Herein, the results of a systematic reevaluation of this phenomenon at potentials up to 5.0 V vs. Li^+/Li, using different carbonate electrolytes containing $LiPF_6$, LiFSI or LiTFSI, are presented. The anodic dissolution is most likely caused by etching of the Al_2O_3 passive layer by protons released during the oxidation of the solvent. This sparks off a second oxidation step, involving the oxidation of the aluminum. While a passive AlF_3 layer is formed in 1.0 M $LiPF_6$, extensive anodic dissolution of aluminum is seen in 1.0 M LiFSI or LiTFSI at potentials where the solvent undergoes oxidation. In 5.0 M LiFSI, a passive layer of AlF_3 is, however, formed most likely due to the presence of fluoride as an impurity in the LiFSI. No significant improvement was seen when using carbon-coated aluminum electrodes.

1. Introduction

Lithium-ion (Li-ion) batteries are of significant importance due to their use in portable devices and electric vehicles. Since the energy density of Li-ion battery is proportional to the operating cell voltage, there is currently a large research interest in high-voltage Li-ion batteries and hence high-voltage positive electrode materials. (Armand et al., 2020; Pender et al., 2020) The use of such electrode materials can, however, give rise to problems concerning the stability of the positive electrode current collector. In Li-ion batteries, aluminum (Al) foil is typically used as the positive electrode current collector material due to aluminum's good mechanical properties and electrochemical stability up to about 3 V (vs. Li^+/Li). (Guo et al., 2021; Zhu et al., 2021; Gabryelczyk et al., 2021; Whitehead and Schreiber, 2005) This stability stems from the presence of a thin native Al_2O_3 surface layer which prevents oxidation of the Al present underneath. (Myung et al., 2011) Since the Al^{3+} present in the Al_2O_3 should not undergo any oxidation, the Al_2O_3 layer should in fact remain stable also at potentials higher than 3 V (vs. Li^+/Li). Nevertheless, the Al_2O_3 layer has been found to deteriorate at such potentials, particularly in electrolytes containing LiFSI or LiTFSI. This effect can then cause anodic dissolution of the Al current collector, which ultimately may lead to a failure of the battery. (Pender et al., 2020; Zhu et al., 2021; Whitehead and Schreiber, 2005; Myung et al., 2011) To be able to circumvent this problem, the reasons for the degradation of the Al_2O_3 passive layers present on the Al current collectors in high-voltage Li-ion batteries clearly need to be identified.

The abovementioned anodic dissolution of the Al current collector has been explained based on various hypotheses. (Gabryelczyk et al., 2021; Myung et al., 2011; Ma et al., 2017; Gao et al., 2018; Solchenbach et al., 2018; Meister et al., 2017; Krämer et al., 2013) For electrolytes containing fluorinated salts (e.g., $LiPF_6$ or $LiBF_4$), (Zhang and Devine, 2006; Zhang et al., 2002) or fluorinated solvents (e.g. methyl difluoro acetate), (Kawamura et al., 2005) passivation is generally obtained due to the formation of an AlF_3 containing surface layer. This layer results from a reaction between Al^{3+} and the HF or F^- formed due to the reaction of PF_6^- with traces of water. (Markovsky et al., 2010) However, in electrolytes containing imide (e.g., $TFSI^-$ and FSI^-) or perchlorate anions no such passivation is seen, which results in rapid anodic dissolution of the Al current collector. (Zhang and Jow, 2002; Morita et al., 2003; Wu and Du, 2021) The high rates of Al anodic dissolution seen in electrolytes containing LiTFSI or LiFSI, have been explained by the higher solubilities of the $Al(TFSI)_x$ and $Al(FSI)_x$ complexes compared to that of AlF_3. This hypothesis is supported by the fact that passivation can be obtained after adding e.g., $LiPF_6$ to an electrolyte containing LiTFSI or LiFSI. (Gabryelczyk et al., 2021; Myung et al., 2011) The onset of anodic dissolution of Al that can be seen at potentials above about 3 V vs. Li^+/Li can, however, clearly not be explained by the HF already present in the electrolyte prior to the start of the electrochemical experiment. This is particularly evident when PF_6^- is present in the electrolyte since PF_6^- then can react with residual water to give HF which then can react with Al_2O_3

* Corresponding authors.
E-mail addresses: leif.nyholm@kemi.uu.se (L. Nyholm), ahmed.etman@kemi.uu.se (A.S. Etman).

https://doi.org/10.1016/j.ces.2023.119346
Received 12 June 2023; Received in revised form 13 September 2023; Accepted 27 September 2023
Available online 29 September 2023

to yield a passive layer containing AlF_3 (i.e., $Al_2O_3 + 6\ HF = 2\ AlF_3 + 3\ H_2O$). The experimental results hence indicate that the dissolution of the Al_2O_3 passive layer seen above 3 V vs. Li^+/Li is likely to be caused by an electrochemical reaction giving rise to the release of protons. (Ma et al., 2017) Since it is known that the organic solvents can undergo oxidations at potentials above 3 V vs. Li^+/Li, (Ma et al., 2017; Gao et al., 2018; Metzger et al., 2020) and that the oxidation of ethylene carbonate (EC) can give rise to a release of protons, it is reasonable to assume that the dissolution of the Al_2O_3 passive layer (and subsequently the anodic dissolution of Al) is initiated by the oxidation of the carbonate solvent (s). (Ma et al., 2017; Gao et al., 2018; Solchenbach et al., 2018; Meister et al., 2017; Krämer et al., 2013) If the observed anodic dissolution of Al is coupled to the oxidation of the carbonate solvent(s), the choice of solvent may then affect the Al anodic dissolution rate depending on their oxidation potentials and oxidation mechanisms.

The dielectric constant of the solvents may also influence the Al anodic dissolution rates via the solubilities of the generated Al^{3+} complexes. (Wang et al., 2000) Moreover, it has been reported that the use of highly concentrated solutions of different salts can suppress the Al anodic dissolution rates by decreasing the number of the free solvent molecules that can solvate the Al^{3+} ions. (Matsumoto et al., 2013) This effect (i.e., the high salt concentration effect) could, however, also be due to a decreased solubility of the Al^{3+} species, caused by the high ionic strength. Since the choice of solvent as well as lithium salt should affect the anodic dissolution rate Al, it is important to systematically study the electrochemical performance of Al_2O_3 passivated Al foils in the most commonly used Li-ion battery carbonate electrolytes at potentials above 3 V vs. Li^+/Li.

As indicated above, the native Al_2O_3 layer protecting the Al foil (which is only a few nanometers thick (Bizot et al., 2021; Strohmeier, 1990) can start to undergo dissolution if protons are generated at the surface of the Al foil during the oxidation of the carbonate solvent(s). (Ma et al., 2017; Gao et al., 2018; Solchenbach et al., 2018; Meister et al., 2017; Krämer et al., 2013) One possibility to slow down this reaction would then be to coat the Al surface with a protective layer that either is thick enough to extend the life-time of the Al current collector sufficiently, or prevents the anodic dissolution reactions from taking place. It has, for example, been shown that carbon-coated Al foils show lower Al anodic dissolution rates compared to bare Al foils, especially in imide electrolytes. (Bizot et al., 2021) Decreased Al anodic dissolution rates have also been found when using graphene-based coatings. (Zhang et al., 2020; Li et al., 2019; Richard Prabakar et al., 2013; Cho et al., 2021) In addition, a surface layer of fumed silica nanoparticles has been found to decrease the Al anodic dissolution rates in LiTFSI electrolytes. (Li et al., 2004) Phosphate based coatings such as $AlPO_4$ (Gao et al., 2018) and $LiPO_2F_2$ (Kim et al., 2022) have likewise been reported to slow down the Al anodic dissolution process, although the reason for this remains unclear. While most of the previous studies have focused on demonstrating the effect of the coatings during relatively few cycles, it is still not clear if the Al anodic dissolution rate for e.g., a carbon coated Al foil, remains sufficiently low during long-term cycling. This is clearly an important question in conjunction with high-voltage Li-ion batteries, given that carbon is thermodynamically unstable at potentials above about 3 V vs. Li^+/Li. Studies therefore need to be carried out to investigate if there are redox reactions involving the carbon coatings at potentials above 3 V vs. Li^+/Li and if these are likely to result in a gradual loss of the carbon coating.

This work discusses the results of a systematic study of the anodic dissolution of 12 μm-thick Al foil in different carbonate electrolytes containing different concentrations of $LiPF_6$, LiTFSI or LiFSI. Voltammetric experiments are performed with lithium-metal electrode-based half cells at a scan rate of 0.5 mV s^{-1} by either scanning the potential of the Al foil from the open circuit potential (OCP) to 5.0 vs. Li^+/Li, or by first scanning from the OCP to 5.0 V and then back to 3 V vs. Li^+/Li. The surfaces of the pristine and cycled Al foils are analyzed with SEM and XPS. The results indicate that the Al_2O_3 passive layer undergoes etching as a result of an oxidation of the solvents generating protons at the electrode surface. This oxidation of the solvents may then be followed by a second oxidation step involving the anodic dissolution of Al. The influence of this two-step oxidation mechanism is studied using different combinations of solvents (i.e., ethylene carbonate (EC), dimethyl carbonate (DMC), diethyl carbonate (DEC), and ethyl methyl carbonate (EMC)), different concentration of salts (i.e., $LiPF_6$, LiTFSI and LiFSI), electrolyte volumes, voltammetric scan rates and cycle numbers. The long-time cycle performance of a carbon-coated Al foil is also investigated as its use could be expected to be advantageous particularly in electrolytes containing LiTFSI or LiFSI. The influence of the high-potential redox reactions involving carbon on the life-time of the carbon coating is likewise discussed.

2. Results and discussion

2.1. Structure and morphology of the employed 12 and 20 μm thick Al foils

In a Li-ion battery, it is important to decrease the mass and volume of the passive components (e.g., the current collectors and the separator) as this will increase the specific energy density of the battery. One way of accomplishing this is to decrease the thickness of the Al current collector used in the positive electrode. The experiments carried out in this study were therefore performed both with an Al foil with a thickness of 12 μm and a foil with a thickness of 20 μm. The XRD patterns obtained for these foils can be seen to be analogous in Fig. 1a. The analysis of the SEM cross-section images (Fig. 1b), which was used to verify the 12 μm thickness of the foil, indicated that the surface of the foil was free from pits and impurities. This is more clearly seen in the top-view SEM image presented in Fig. S1a in the Supporting Information.

2.2. Electrochemical performance of the Al foils in carbonate electrolytes containing $LiPF_6$

The electrochemical performances of the Al foils were studied in lithium-metal-based half cells typically using linear sweep voltammetry (LSV) or cyclic voltammetry (CV) at a scan rate 0.5 mV s^{-1}. In the LSV case, the potential was scanned from the OCP (i.e., about 2.1 to 2.2 V vs. Li^+/Li) to 5.0 V vs. Li^+/Li, whereas a reverse scan to 3.0 V vs. Li^+/Li was included in the CV experiments. In Fig. 1c, an increase in the oxidation current density is seen at about 3.0 V vs. Li^+/Li for both Al-foils in the electrolyte composed of 1.0 M $LiPF_6$ dissolved in 1:1 EC:DEC. Although a larger increase in the current density was initially seen for the 20 μm thick foil than for the 12 μm thick Al one, the current densities reached at 5.0 V vs. Li^+/Li were approximately the same. Analogous results were also found for the 20 μm and 12 μm thick Al foils in 5.0 M LiFSI dissolved in DMC as can be seen in Fig. 1d. The similarities between the electrochemical performances of the two Al foils were expected, since both foils were prepared with rolling processes and hence feature similar surface striations. (Kerry, 2012; Zhang and Devine, 2006) As a result the in-depth discussion of the oxidation behaviors in the two electrolytes will mainly be focused on the results obtained with the 12 μm thick Al foil.

The voltammograms obtained for the Al foils in 1.0 M $LiPF_6$ dissolved in 1:1 EC:DEC seen in Fig. 1c clearly show the onset of an oxidation reaction at about 3.0 V vs. Li^+/Li. Since the surfaces of the pristine Al-foils were coated with native Al_2O_3 passive layers (see Fig. 1e), the oxidation onset at about 3 V vs. Li^+/Li is very unlikely to have been caused by the oxidation of Al. The oxidation of Al to Al_2O_3 or AlF_3 should, incidentally, take place already at about 0.14 and 0.97 V vs. Li^+/Li according to thermodynamics (see the Supporting Information Note S1). An oxidation of the Al(III) in the Al_2O_3 layer can also be excluded as Al(III) is the highest Al oxidation state. As will be discussed below, an oxidation of the oxygen in the Al_2O_3 (yielding O_2) is likewise unlikely at about 3 V vs. Li^+/Li. For 1.0 M $LiPF_6$ dissolved in 1:1 EC:DEC, an oxidation of Li^+ is also very unlikely. An oxidation of PF_6^- is likewise

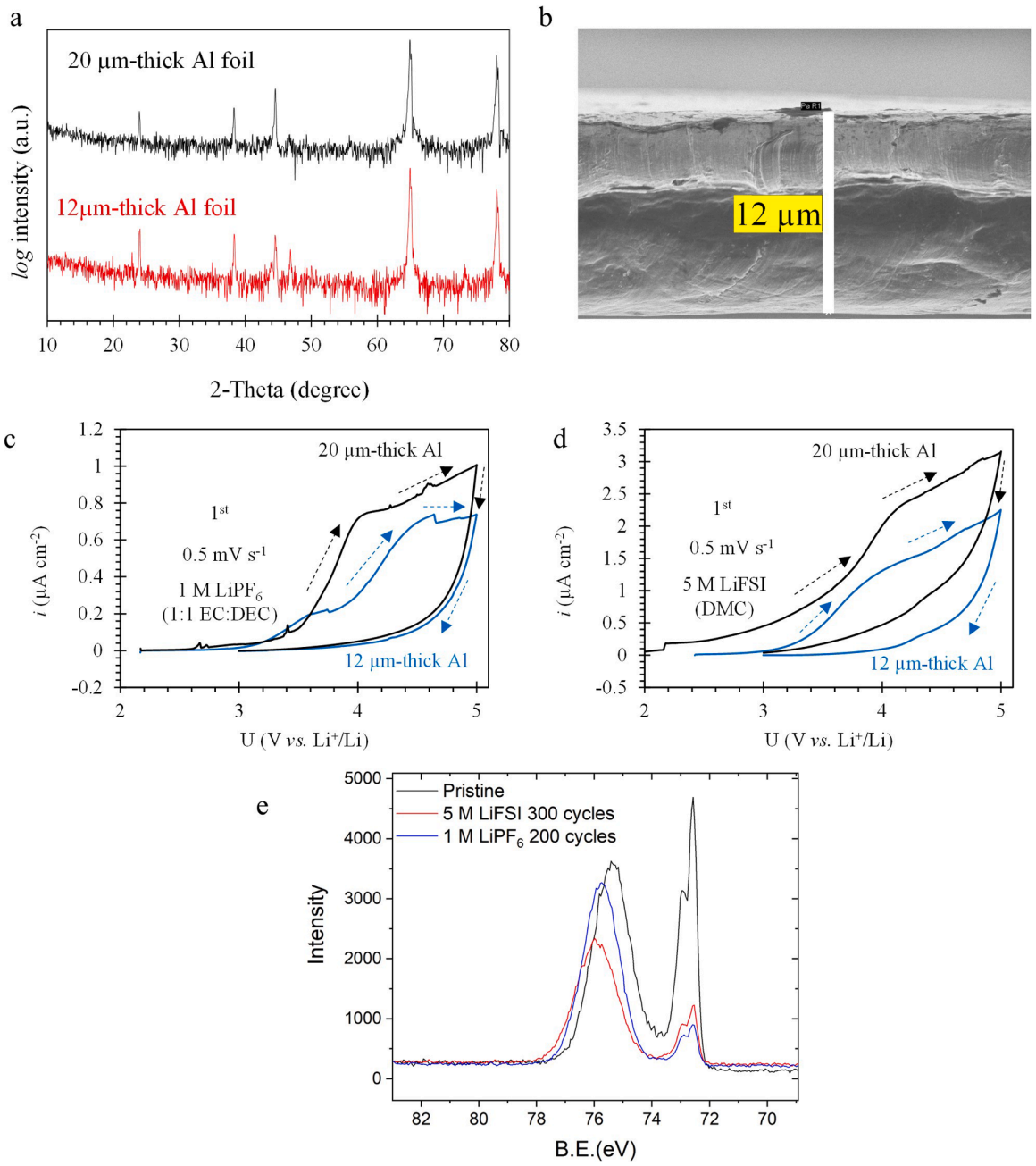

Fig. 1. Structure, morphology, and electrochemical performance of the 12 and 20 µm thick Al foils: (a) XRD patterns and (b) and SEM-cross-section image of the 12 µm thick foil. (c) and (d) cyclic voltammograms recorded at a scan rate of 0.5 mV s^{-1} for the 12 µm-thick (blue) and 20 µm-thick (black) Al foil in the 1.0 M $LiPF_6$ EC:DEC (1:1) and 5.0 M LiFSI in DMC (1:1) electrolytes, respectively. (e) Al 2p XPS spectra for a pristine 12 µm thick Al foil (black curve) and a 12 µm thick Al foil after extended cycling in 1.0 M $LiPF_6$, EC:DEC (1:1), (blue curve) and 5.0 M LiFSI, DMC, (red curve), respectively. (For interpretation of the references to colour in this figure legend, the reader is referred to the web version of this article.)

improbable given that the fluoride oxidation state is (-I) and the phosphorous oxidation state is (+V). This means that the oxidation at about 3 V vs. Li^+/Li in 1.0 M $LiPF_6$ (dissolved in 1:1 EC:DEC) must have been due to another redox reaction. As will be shown below, the most likely explanation is then that (at least) EC is oxidized, as it is has been shown (Ma et al., 2017) that EC can be oxidized in this potential region.

The shapes of the voltammogram in Fig. 1c also indicate that surfaces of the Al foils were gradually passivated during the scan from 3.0 to 5.0 V vs. Li^+/Li. For the 12 µm thick Al foil, this is clearly seen as the current density became approximately constant at potentials above about 4.5 V vs. Li^+/Li. Al 2p XPS spectra for the Al foil obtained before and after the cycling for 200 cycles in 1.0 M $LiPF_6$ EC:DEC are shown in Fig. 1e. The peaks observed at binding energies of about 72.6 eV and 75.4 eV can be assigned to metallic Al and Al_2O_3, respectively. Based on the ratio between the metallic Al and Al_2O_3 peak areas, (Strohmeier, 1990; Carlson and McGuire, 1972) the thickness of the native Al_2O_3 layer was found to be about 3 to 4 nm. As a result of the cycling in the 1.0 M $LiPF_6$ EC:DEC electrolyte, the peak associated with non-metal Al was shifted from 75.4 eV to 76.0 eV (see Fig. S1b), which indicates bonding of Al^{3+} to the more electronegative fluoride (e.g. Al—F or Al—O—F) yielding a passive layer containing AlF_3 and/or aluminium oxy-fluoride. This observation agrees well with previous findings indicating that an AlF_3 layer is formed on top of the Al_2O_3 layer, although no separate peaks can be easily distinguished in the present case. (Ma et al., 2017; Gao et al.,

2018; Zhang and Devine, 2006; Zhang and Devine, 2006) The change in the ratio between the areas of the metallic Al and non-metal peak (i.e., Al—F and/or Al—O—F) suggests that the thickness of the layer was about 6 to 8 nm (assuming pure Al_2O_3 or pure AlF_3). This hence means that there was an increase in the thickness as well as a possible change in the composition of the layer during the cycling in the 1.0 M $LiPF_6$ EC:DEC electrolyte. It should be noted that the prediction of the passive layer composition using the binding energy of the non-metal peak is not straightforward because the binding energy can also be affected by several other factors, such as the measurement procedure (Baer et al., 2020), thickness of the layer (Baer et al., 2002) and possible built-in charges (Lindgren et al., 2017). Further details regarding this are summarized in Supporting Information XPS–Note. Note also, that the top layers are assumed to be sufficiently thin to allow the Al metal peak to be used as a binding energy reference.

When the Al-foils were subjected to repeated cycling between 3.0 and 5.0 V vs. Li^+/Li in 1.0 M $LiPF_6$ (dissolved in 1:1 EC:DEC), a notable passivation effect was seen already on the second cycle (see Fig. 2a). This yielded a significantly decreased oxidation current density between 3.0 and 5.0 V vs. Li^+/Li. On the 85th cycle the oxidation current density was even lower. Moreover, no significant difference could be seen between the shapes of the voltammograms recorded on the 85th and 300th cycle (see Fig. S2a in the Supporting Information). These findings demonstrate that the Al-foil remained passivated even during long-term cycling in the 1.0 M $LiPF_6$ EC:DEC (1:1) electrolyte, in very good agreement with previous findings. (Zhang and Devine, 2006; Bizot et al., 2021; Zhang and Devine, 2006; Myung et al., 2009) Moreover, the analysis of top-view surface and cross-section images SEM images obtained after cycling for about 300 cycles (see Fig. 2c) failed to indicate any pits or cracks on the surface of the Al foil. As mentioned above, the observed passivation can be explained by the formation of an AlF_3 layer on top of the native Al_2O_3 layer. (Ma et al., 2017; Gao et al., 2018; Zhang and Devine, 2006; Zhang and Devine, 2006) Since the native Al_2O_3 layer should be stable at the employed potentials, the question is then how the AlF_3 surface layer was formed on top of the Al_2O_3 layer?

When trying to answer this question one should first examine the first cycle voltammograms in more detail. In Fig. 2a, it can be seen that the oxidation in fact involved a two-step reaction in 1.0 M $LiPF_6$ dissolved in EC:DEC since two overlapping oxidation steps are seen at about 3.2 and 3.7 V vs. Li^+/Li, respectively. Another interesting observation is that the shape of the first cycle voltammogram depended on the employed scan rate. When decreasing the scan rate from 0.5 to 0.05 mV s^{-1}, the first wave became more prominent, and an approximately constant current density was also seen above 3.5 V vs. Li^+/Li. The latter observation together with the onset of the second oxidation step at about 3.3 V vs. Li^+/Li, yielding an oxidation peak at about 3.4 V vs. Li^+/Li, suggest that a passive layer was formed on the electrode surface during the first cycle when using the lower scan rate, i.e., 0.05 mV s^{-1} (see also the second 0.05 mV s^{-1} cycle in Fig. S1c). In contrast, in Fig. 2a it can be seen that an oxidation was still seen on the second cycle for a scan rate of 0.5 mV s^{-1}. The formation of the passive layer was hence incomplete on the first cycle when using a scan rate of 0.5 mV s^{-1}, most likely due to the ten times shorter cycle time. This hypothesis is further supported by the fact that the first cycle oxidation charges between 3.0 and 5.0 V vs. Li^+/Li were found to be about 1.2 mC when scanning at 0.5 mV s^{-1} and 5.8 mC when scanning at 0.05 mV s^{-1}, respectively. It can therefore be concluded that a passive layer is formed on the Al electrode in the 1.0 M $LiPF_6$ EC:DEC electrolyte provided that the oxidation is allowed to proceed for a sufficiently long time. The possible reasons for this behavior will be discussed below.

As already indicated above, the first oxidation step most likely involved an oxidation of the solvent(s), (Gabryelczyk et al., 2021; Ma et al., 2017; Gao et al., 2018; Solchenbach et al., 2018; Meister et al., 2017; Krämer et al., 2013) i.e., EC and/or DEC. This should result in a

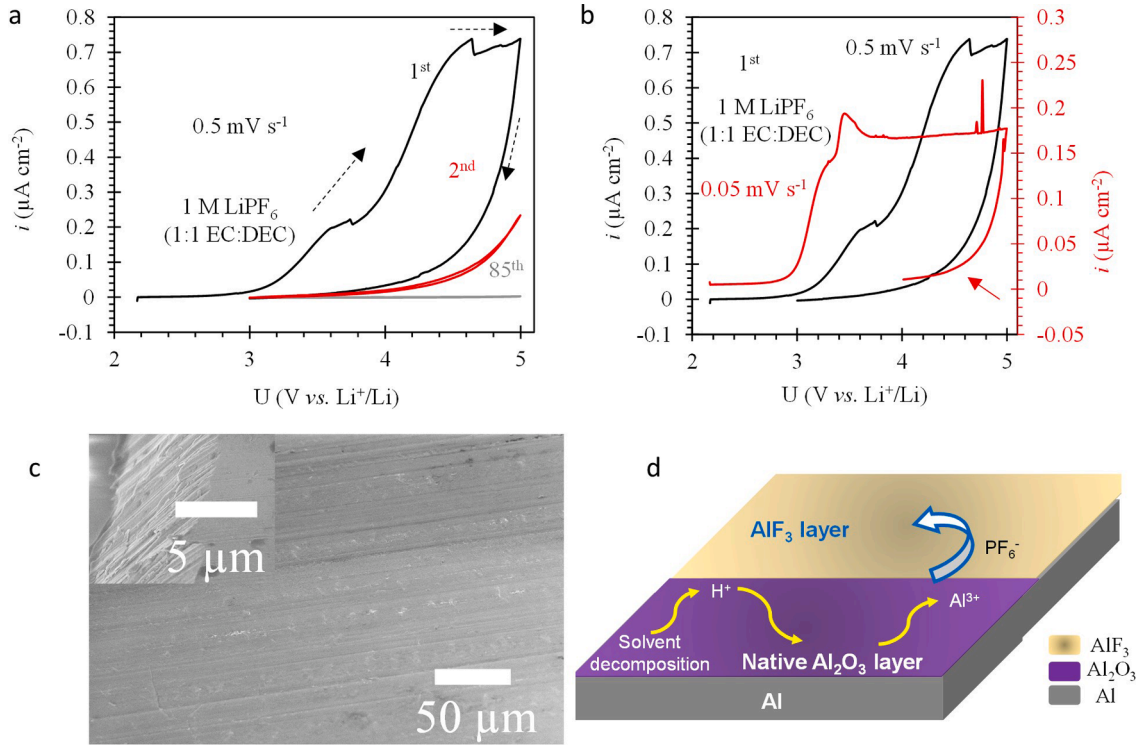

Fig. 2. The performance of 12 µm thick Al foils in carbonate electrolytes containing $LiPF_6$: (a) cyclic voltammograms recorded in a 1.0 M $LiPF_6$ EC:DEC electrolyte at a scan rate of 0.5 mV s^{-1} where the arrows show the scan direction. (b) Comparison of first cycle voltammograms recorded in the 1.0 M $LiPF_6$ EC:DEC electrolyte at scan rates of 0.5 (black curve) and 0.05 (red curve) mV/s, respectively. (c) SEM images of the Al foil obtained after extended cycling (~300 cycles) in the 1.0 M $LiPF_6$ EC:DEC electrolyte. (d) Schematic illustration of the two-step oxidation process occurring in a carbonate electrolyte containing $LiPF_6$. (For interpretation of the references to colour in this figure legend, the reader is referred to the web version of this article.)

release of H^+ at the surface of the Al foil (see Reaction (1). If the local concentration of H^+ at the electrode surface becomes high enough, there are then two possible reaction pathways. In the first case, the generated H^+ attacks the Al_2O_3 layer causing it to undergo dissolution (Reaction (2a). This reaction should be spontaneous under standard conditions, see the Supporting Information Note S2). The generated Al^{3+} then reacts with PF_6^- to form AlF_3 on the surface of the Al-foil (Reaction (2b). Reaction (2b) should likewise be spontaneous (under standard conditions) as the dissociation of PF_6^- into PF_5 and F^- is spontaneous as well as the formation of AlF_3 from Al^{3+} and F^- (see the Supporting Information Note S2). In the second case, the H^+ generated in Reaction (1) first reacts with PF_6^- to generate HF (Reaction 3a) after which the HF reacts with Al_2O_3 to generate AlF_3 according to Reaction 3b. Both the combination of Reactions (2a) and b, and the combination of Reactions 3a and b, however, give rise to the same total reaction, i.e., Reaction 4. It is therefore reasonable to assume that a sufficiently large release of H^+, e.g., as a result of an oxidation of the EC, results in a formation of AlF_3 on top of the Al_2O_3 layer in agreement with previous findings. (Ma et al., 2017; Gao et al., 2018; Zhang and Devine, 2006; Zhang and Devine, 2006) Unlike Al_2O_3, the AlF_3 should not react with H^+ under standard conditions as the reaction $AlF_3 + 3H^+ = Al^{3+} + 3HF$ then is thermodynamically unfavorable (see the Supporting Information Note S2). This explains why a passivation of the electrode is seen once AlF_3has been formed on the surface of the electrode. A complete dissolution of the Al_2O_3 layer as a result of Reaction 4 is unlikely as the formed AlF_3 layer should protect the Al_2O_3 underneath. This hypothesis in good agreement with previous findings. (Ma et al., 2017; Gao et al., 2018; Zhang and Devine, 2006; Zhang and Devine, 2006) as well as the XPS results discussed above. The passivation of the Al foil is schematically summarized in Fig. 2d.

At this point it should be recalled that as Reactions 2a and 3b are equilibrium reactions, the etching of Al_2O_3 by H^+ (or HF) should only take place if the concentration of H^+ (or HF) at the electrode surface is high enough. This means that if the rate of the oxidation of the solvent(s) were to decrease sufficiently, the decrease in the local concentration of H^+ (or HF) at the electrode surface may allow Al_2O_3 to be reformed as a passive layer on the aluminum electrode (see below). This indicates that the anodic dissolution of aluminum is driven by the oxidation of the solvent(s), as previously proposed. (Ma et al., 2017; Gao et al., 2018; Solchenbach et al., 2018; Meister et al., 2017; Krämer et al., 2013)

$$\text{Carbonate solvent} \rightarrow \text{Oxidized carbonate solvent} + x\,H^+ + x\,e^- \quad (1)$$

$$6\,H^+ + Al_2O_3 \leftrightarrow 3\,H_2O + 2\,Al^{3+} \quad (2a)$$

$$2\,Al^{3+} + 6\,PF_6^- \leftrightarrow 6\,PF_5 + 2\,AlF_3 \quad (2b)$$

$6H^+ + 6\ PF_6^- \leftrightarrow 6\ PF_5 + 6HF$ (3a).

$Al_2O_3 + 6\ HF \leftrightarrow 2\ AlF_3 + 3\ H_2O$ (3b).

$Al_2O_3 + 6H^+ + 6\ PF_6^- \leftrightarrow 2\ AlF_3 + 6\ PF_5 + 3\ H_2O$ (4).

Although Reaction 4 can explain the formation of a passive layer composed of a mixture of AlF_3 and Al_2O_3 on Al electrodes cycled in the 1.0 M $LiPF_6$ EC:DEC electrolyte, it cannot explain the shapes of the voltammograms seen in Figs. 1 and 2. This is particularly evident when looking at the second oxidation step, which appears to result in passivation of the electrode, in the 0.05 mV s^{-1} voltammogram in Fig. 2b. As Reaction 4 should stop once the Al_2O_3 layer has been coated with a layer of AlF_3 it is also unlikely that the Al_2O_3 layer was completely replaced by an AlF_3 layer. It can therefore be concluded that the oxidation of the solvent must have been accompanied by another oxidation resulting in growth of the AlF_3 layer. Further support for this hypothesis can be gained by assuming that the oxidation of the solvent was responsible for the current density between 2.8 and 3.3 V vs. Li^+/Li (see the red curve in Fig. 2b). The solvent oxidation charge would then be about 1.1 mC, which would correspond to a sufficient amount of H^+ to convert a 0.6 nm thick Al_2O_3 layer into a 1.4 nm thick AlF_3 layer (see the Supporting Information Note S3 and Note S4). The formed AlF_3 layer should in fact be thinner as some of the H^+ would diffuse into the electrolyte and therefore not react with the Al_2O_3. Here it should also be mentioned that the amount of solvent consumed in the solvent oxidation step (see the red curve in Fig. 2b) should have been negligible in comparison with the total amount of solvent present in the cell (i.e., of the order of 10 nmol or about $1{\cdot}10^{-3}$ % of the total amount of solvent present in the electrolyte, see the Supporting Information Note S5).

Given the oxidation peak at about 3.4 V vs. Li^+/Li and the subsequent constant current density up to 5.0 V vs. Li^+/Li seen in the 0.05 mV s^{-1} voltammogram in Fig. 2b, it is reasonable to assume (as is further explained below) that the second oxidation step involved oxidation of the Al electrode at the Al/Al_2O_3 interface as suggested by Reaction 5. In this reaction, the so generated Al^{3+} reacts with F^- to yield AlF_3. The presence of this reaction, which would be initiated by the etching of the Al_2O_3 layer, also suggests that an AlF_3 layer needs to be thicker than an Al_2O_3 layer in order to be passive. The Al^{3+} generated at the Al surface would then migrate through the passive layer towards the interface between the passive film and the electrolyte while the F^- would migrate in the opposite direction. (Zhang and Devine, 2006; Zhang and Devine, 2006; Yoon et al., 2022) The fluoride must then stem from the PF_6^- present in the electrolyte as a result of the $PF_6^- \leftrightarrow PF_5 + F^-$ (e.g., Reaction 3a) (Zhang and Devine, 2006; Stich et al., 2018) which would be shifted to the right when fluoride is consumed due to the formation of HF and/or AlF_3. The thickness of the AlF_3 layer should then increase as the oxidation potential is increased (Zhang and Devine, 2006; Zhang and Devine, 2006) which would explain the constant current density seen between 3.6 and 5.0 V vs. Li^+/Li seen for the red curve in Fig. 2b.

$Al + 3F^- \rightarrow AlF_3 + 3\ e^-$ (5).

The thickness of the generated AlF_3 layer can then be estimated if the second oxidation charge is known. For the 0.05 mV s^{-1} scan rate (see Fig. 2b), the charge associated with the second oxidation was about 4.7 mC (i.e., the total first cycle oxidation charge, 5.8 mC, minus the first cycle solvent oxidation charge, 1.1 mC). This oxidation charge indicates that an about 6 nm thick AlF_3 layer should have been formed on the first cycle (see the Supporting Information Note S3 and Note S4). The passive layer present after cycling to 5.0 V vs. Li^+/Li on the first cycle should consequently have been composed of about 6 nm AlF_3 and about 2 to 3 nm of Al_2O_3 (i.e., 3 to 4 nm minus the 0.6 nm lost as a result of Reaction 4). This total thickness of about 8 to 9 nm is in good agreement with the thickness of 6 to 8 nm suggested by the abovementioned XPS results.

The second oxidation is thus unlikely to have stemmed from an oxidation of the water generated in Reaction 4 since such an oxidation (see Reaction (6) should not give rise to any passivation. The generated water would most likely react either with the simultaneously formed PF_5 or with POF_3 according to Reactions (7) and (8). (Solchenbach et al., 2018; Stich et al., 2018) Alternatively, the water may undergo reduction at the lithium electrode.

$$2\,H_2O \rightarrow 4\,H^+ + 4\,e^- + O_2 \quad (6)$$

$$H_2O + PF_5 \leftrightarrow POF_3 + 2\,HF \quad (7)$$

$$POF_3 + H_2O \leftrightarrow HPO_2F_2 + HF \quad (8)$$

An oxidation of the O^{2-} in the Al_2O_3 according to Reaction (9) (Gabryelczyk et al., 2021) is likewise unlikely as it should only be thermodynamically possible at potentials above about 4 V vs. Li^+/Li (see the Supporting Information Note S1) whereas the onset of the second oxidation step was seen already at about 3.3 V vs. Li^+/Li (see Fig. 2b.).

$$Al_2O_3 \rightarrow 3/2\,O_2 + 2\,Al^{3+} + 6\,e^- \quad (9)$$

When comparing the shapes of the 0.05 and 0.5 mV s^{-1} voltammograms in Fig. 2b, it is seen that the lower scan rate resulted in less drawn-out oxidation reactions as well as a relatively large solvent oxidation charge. This indicates that the formation of the passive layer benefitted from an extension of the time during which the solvent was oxidized. It is then reasonable to assume that the faster AlF_3 passivation was a result

of the presence of larger amounts of HF (i.e., F^-) at the electrode surface, see Reactions 3a and b. The results thus demonstrate that the AlF_3 containing passive layer formed as a result of Reactions 4 and 5 prevented further oxidation of the solvent. The long-time stability of the AlF_3 containing passive layer should then depend on the solubility of AlF_3 and the possibility to generate new AlF_3 via Reaction 5. Based on the discussion above, the possible reactions for the observed first oxidation and second oxidation steps can be schematically presented as shown in Fig. 3a and b, respectively.

Based on the voltammograms presented in Figs. 1 and 2 and the discussion above, it is reasonable to assume that, at least the EC, in the 1.0 M $LiPF_6$ EC:DEC electrolyte underwent oxidation above about 3 V vs. Li^+/Li. The question is then if analogous oxidations also are seen for other commonly employed carbonate solvents. Although the anodic dissolution of Al has been studied in many carbonate solvents, (Zhang and Devine, 2006; Morita et al., 2003; Zhang et al., 2005; Kramer et al., 2012) the influence of the type of carbonate solvent on the anodic dissolution of Al is still not immediately clear. To investigate this, the electrochemical performance of 12 μm thick Al foil electrodes was studied in five different carbonate electrolytes containing $LiPF_6$ salt, i.e., 1.0 M $LiPF_6$ EC/DEC (1:1), 1.0 M $LiPF_6$ EC/DMC (1:1), 1.0 M $LiPF_6$ DEC, 1.0 M $LiPF_6$ DMC, and 1.2 M $LiPF_6$ EC/EMC (3:7). As can be seen in Fig. 3c, analogous first cycle voltammograms were obtained in all cases with respect to the maximum anodic current densities (which ranged from 0.6 to 1.6 μA cm^{-2}) and onset potentials (see Table 1). The two oxidation steps can also be more or less clearly seen for all five electrolytes. For all the $LiPF_6$ containing electrolytes, a passivation was found to take place during the first few cycles (see Fig. S2b-e). This is in excellent agreement with the results discussed above, as well as previous results. (Ma et al., 2017; Morita et al., 2003; Cho et al., 2021; Zhang and Devine, 2006) It is therefore reasonable to assume that all the studied carbonate solvents underwent similar types of oxidations and that this resulted in a release of H^+ at potentials above about 3 V vs. Li^+/Li.

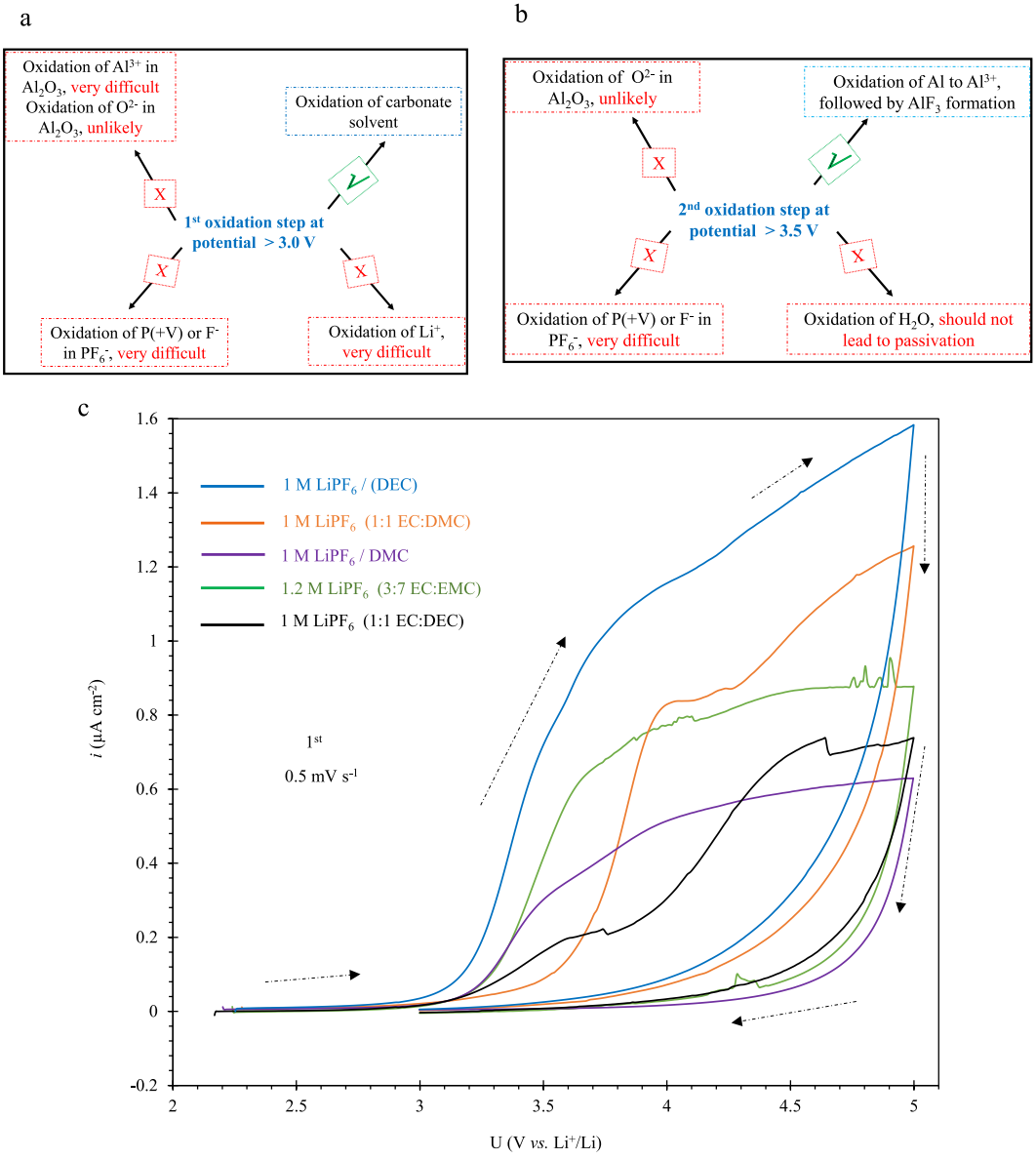

Fig. 3. (a) and (b) schematic illustrations of the reactions that could yield the observed first and second oxidation steps, respectively. (c) Comparison of the first cycle cyclic voltammograms for 12 μm thick Al foils in carbonate electrolytes containing $LiPF_6$: 1.0 M $LiPF_6$ EC/DEC (black), 1.0 M $LiPF_6$ EC/DMC (orange), 1.0 M $LiPF_6$ DEC (blue), 1.0 M $LiPF_6$ DMC (purple), and 1.2 M $LiPF_6$ EC/EMC (green). The arrows indicate the scan direction. (For interpretation of the references to colour in this figure legend, the reader is referred to the web version of this article.)

Table 1
The onset oxidation potentials and degree of passivation seen for the 12 μm Al foil and a carbon-coated Al foil in different carbonate electrolytes.

Electrode	Electrolyte (50 μl)	Oxidation onset	Passivation
Al (20 μm)	1 M $LiPF_6$ in 1:1 EC/DEC, (LP40)	3.35 V	Yes
	5 M LiFSI in DMC	3.13 V	Yes
Al (12 μm)	1 M $LiPF_6$ in 1:1 EC/DEC, (LP40)	3.25 & 3.70 V	Yes
	1 M $LiPF_6$ in 1:1 EC/DMC	3.36 V	Yes
	1.2 M $LiPF_6$ in 1:1 EC/EMC	3.20 V	Yes
	1 M $LiPF_6$ in DMC	3.20 V	Yes
	1 M $LiPF_6$ in DEC	3.10 & 3.60 V	Yes
	1 M LiTFSI in EC/DEC	3.00 & 4.00 V	Further oxidation; passivation after ~ 10 scans
	1 M LiFSI in EC/DMC	3.20 & 4.15 V	Further oxidation; passivation after ~ 10 scans
	1 M LiTFSI in EC/DEC (100 μl)	3.00 & 4.00 V	Further oxidation; passivation after ~ 10 scans
	5 M LiFSI in DMC	3.23 V	Yes
C-coated Al	1 M $LiPF_6$ in 1:1 EC/DEC, (LP40)	3.36 & 3.67 V	Yes
	1 M LiTFSI in EC/DEC (100 μl)	3.60 & 3.80 V	Further oxidation; passivation after ~ 10 scans
	5 M LiFSI in DMC	3.60 V	Yes

2.3. Electrochemical performance of Al foils in carbonate electrolytes containing imide salts

Battery electrolytes containing imide salts such as LiFSI and LiTFSI have been extensively explored as alternatives to $LiPF_6$-based electrolytes, due to concerns regarding the thermal and chemical stability of $LiPF_6$. (Solchenbach et al., 2018; Murmann et al., 2013; Kerner et al., 2016) It is, however, well-known that aluminum electrodes have low electrochemical stabilities at potentials above 3 V vs. Li^+/Li in electrolytes containing LiFSI or LiTFSI (dissolved in carbonate solvents) as a result of the formation of soluble aluminum complexes. (Morita et al., 2003; Wu and Du, 2021; Bizot et al., 2021; Cho et al., 2012) As can be seen in Fig. 4a and b, very high first cycle oxidation current densities (600 – 1800 μA cm^{-2}) were obtained when cycling 12 μm Al foil electrodes in 1.0 M LiFSI EC:DMC (1:1) and 1.0 M LiTFSI EC:DEC (1:1), respectively. The shapes of the voltammograms were also significantly different from those obtained in 1.0 M $LiPF_6$ as the current densities continued to increase after reaching 5.0 V vs. Li^+/Li. This indicates that an activation of the electrode (yielding an increasing electroactive electrode area) took place during the scan, driven by a gradual loss of the native Al_2O_3 passive layer. In this case passivation via the formation of an AlF_3 layer could clearly not take place as there was no PF_6^- (generating fluoride) in the electrolyte.

A comparison of the first cycle voltammograms obtained in 1.0 M $LiPF_6$ EC:DEC (1:1) and 1.0 M LiFSI EC:DMC (1:1) is shown in Fig. 4c. Note the different current scales and that the oxidation onset potential seemed to be higher in the 1.0 M LiFSI EC:DMC (1:1) than in the 1.0 M $LiPF_6$ EC:DEC (1:1) electrolyte. As can be seen in Fig. 4d, showing a magnification of the oxidation onset region, the oxidation onset potentials were, nevertheless, very similar in the 1.0 M LiFSI EC:DMC (1:1), 1.0 M LiTFSI EC:DEC (1:1) and 1.0 M $LiPF_6$ EC:DEC (1:1) electrolytes. In agreement with the $LiPF_6$ results discussed above, two overlapping oxidation steps were also seen in the 1.0 M LiFSI EC:DMC (1:1) and 1.0 M LiTFSI EC:DEC (1:1) electrolytes. In Fig. 4d, the onset of the first oxidation step was found at about 3.0 and 3.2 V in 1.0 M LiTFSI EC:DEC (1:1) and 1.0 M LiFSI EC:DMC (1:1), respectively. Since these potentials are in very good agreement with the corresponding potential for 1.0 M $LiPF_6$ dissolved in EC:DEC (1:1), it is reasonable to assume that the first oxidation step stemmed from the oxidation of the carbonate solvents also in Fig. 4.

Based on the assumed solvent oxidation charges up to 3.9 V for LiTFSI and 4.0 V for LiFSI (i.e., 0.87 and 0.59 mC, respectively,) the amount of H^+ generated should only have been able to etch away a small part of the Al_2O_3 layer (i.e., 0.5 and 0.3 nm in the LiTFSI and LiFSI electrolytes, respectively, see the Supporting Information). Nevertheless, once the thickness of the Al_2O_3 layer started to decrease, the Al oxidation rate should have increased. Since an AlF_3 passive layer could not be formed, a large increase in the current density was seen at about 4.0 and 4.15 V vs. Li^+/Li in 1.0 M LiTFSI dissolved in EC:DEC (1:1) and 1.0 M LiFSI dissolved in EC:DMC (1:1), respectively. These large current densities should stem from solvent oxidation and anodic dissolution of Al. The remaining part of the native Al_2O_3 oxide layer should then be dissolved by the H^+ produced in the oxidation of the solvents whereas the anodic dissolution of Al would generate pits on the electrode surface, resulting in an electroactive area that increased with time. Many pits and holes were consequently seen in the SEM images (see Fig. 5e) recorded after cycling the Al foil in 1.0 M LiTFSI EC:DEC (1:1) for about 300 cycles. Due to the large currents associated with the presumed oxidation of the solvent and the Al electrode seen at potentials above about 4 V vs. Li^+/Li in the LiTFSI and LiFSI electrolytes, it was not possible to establish whether $TFSI^-$ and/or FSI^- likewise underwent oxidation in this potential region.

In Fig. 4a and b it can also be seen that the oxidation current density decreased to about zero at about 3.7 V vs. Li^+/Li on the return scan. This indicates that a re-passivation took place once the rate of the oxidation of the solvents had decreased sufficiently. Since Reaction (2a) is an equilibrium reaction, this effect can be explained by reformation of Al_2O_3 on the Al surface (via $Al^{3+} + 3\ H_2O = Al_2O_3 + 6H^+$) once the concentration of protons at the electrode surface becomes low enough. This hypothesis is further supported by the XPS results depicted in Fig. S1b in the Supporting Information, indicating the presence of a passive layer on an electrode cycled in 1.0 M LiTFSI EC:DEC (1:1). This means that these results are in excellent agreement with the hypothesis that the oxidation of the solvents generates protons which cause the anodic dissolution of the Al_2O_3 coated Al electrodes. In Fig. 4e and f it is seen that the oxidation current density decreased during the first 10 cycles. On the 10th cycle, the oxidation current densities were thus only about 120 μA cm^{-2}, compared to 1000–2000 μA cm^{-2} on the first and second cycles. This indicates that there was a gradual saturation of the electrolyte in the vicinity of the electrode surface with respect to the different Al-species $Al(FSI)_x$ or $Al(TFSI)_x$. The oxidation current density thus became controlled by the rate of the diffusion of the generated Al-species away from the electrode surface. This saturation hypothesis is further supported by the results obtained with different electrolyte volumes which will be discussed below. For the voltammograms shown in Fig. 4e and f, the accumulated irreversible oxidation charges were 5.2 and 5.7 C after the first ten cycles in 1.0 M LiTFSI dissolved in EC:DEC (1:1) and 1.0 M LiFSI EC:DMC (1:1), respectively. Such irreversible capacity losses would clearly be a major problem in Li-ion batteries. It should also be mentioned that the significant anodic dissolution of aluminum should have resulted in significant deposition of aluminum on the Li counter electrode.

As shown in Fig. 5a and b, cycling experiments were likewise carried out in 50 μl and 100 μl of 1.0 M LiTFSI EC:DEC (1:1) to further test the abovementioned saturation hypothesis. While the shapes of the first cycle voltammograms were analogous for both electrolyte volumes, the fourth cycle anodic current densities were found to be significantly higher (i.e., 350 compared to 150 μA cm^{-2}) when an electrolyte volume of 100 μl was used. These results are in good agreement with the saturation hypothesis.

The electrochemical performances of the Al foil electrodes in 1.0 M LiTFSI EC:DEC (1:1) and 1.0 M LiFSI EC:DMC (1:1) can thus be explained based on the two-step oxidation reaction schematically shown in Fig. 5f. As the solvents undergo oxidation at the Al foil surface, there is a release of H^+ which then attack the native Al_2O_3 surface layer. As a

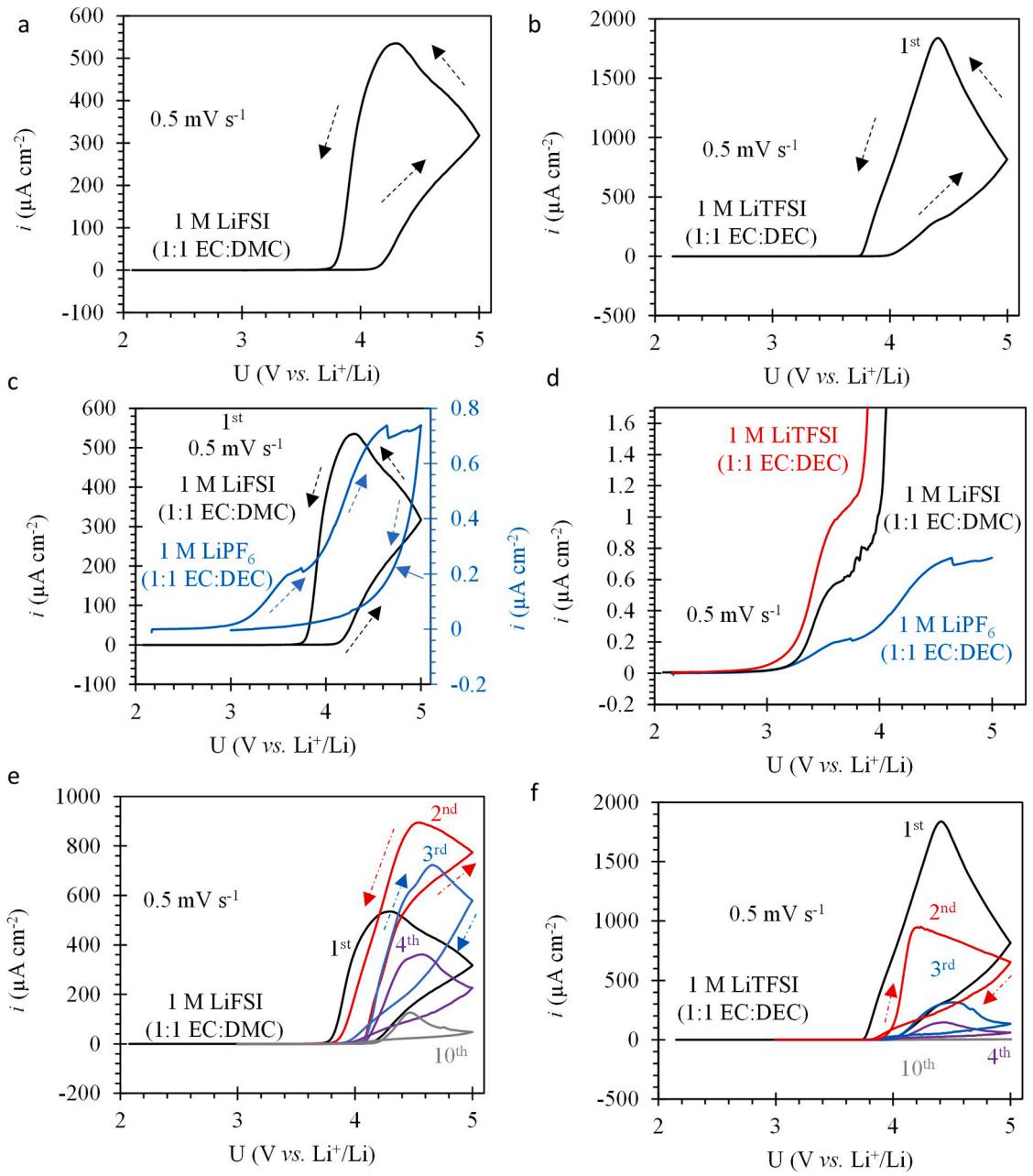

Fig. 4. The electrochemical performance of 12 µm thick Al foil electrodes in carbonate electrolytes containing imide salts: (a) and (b) First cycle cyclic voltammograms recorded at a scan rate of 0.5 mV s^{-1} in 1.0 M LiFSI EC:DMC (1:1) and 1.0 M LiTFSI EC:DEC (1:1) electrolytes, respectively. (c) A comparison of the first cycle cyclic voltammograms recorded at a scan rate of 0.5 mV s^{-1} in 1.0 M LiFSI EC:DMC (1:1) (black curve) and 1.0 M $LiPF_6$ EC:DEC (1:1) (blue curve). Note the different current scales (d) First cycle linear sweep voltammograms recorded at a scan rate of 0.5 mV s^{-1} in 1.0 M LiFSI EC:DMC (1:1) (black curve), 1.0 M LiTFSI EC:DEC (1:1) (red curve) and 1.0 M $LiPF_6$ EC:DEC (1:1) (blue curve). (e) and (f) Cyclic voltammograms showing the 1st, 2nd, 3rd, 4th, and 10th cycles, recorded at a scan rate of 0.5 mV s^{-1} in 1.0 M LiFSI EC:DMC (1:1) and 1.0 M LiTFSI EC:DEC (1:1), respectively. (For interpretation of the references to colour in this figure legend, the reader is referred to the web version of this article.)

result of this, the anodic dissolution of the Al electrode starts, generating pits and holes on the surface of the Al electrode. The generated Al^{3+} ions react with $TFSI^-$ or FSI^- ions to form soluble complexes $Al(TFSI)_x$ and $Al(FSI)_x$. A gradual passivation can then be seen when the solubility of the Al^{3+} complexes in the electrolyte is exceeded first at the electrode surface and then in the entire electrolyte.

2.4. The electrochemical performance of Al foil electrodes in 5.0 M LiFSI dissolved in DMC

It has been reported (Matsumoto et al., 2013; Piao et al., 2021) that imide electrolytes with high salt concentrations can be used to improve the anodic stability of Al foil electrodes. Although this effect has been proposed (Matsumoto et al., 2013; Yamada et al., 2015; Aktekin et al., 2022) to stem from the formation of a LiF layer on the surface of the Al electrode, it is not immediately clear why such a layer would be formed at potentials where there is anodic dissolution of aluminum (generating Al^{3+}). Experiments were therefore performed to study the influence of the LiFSI concentration on the anodic dissolution of aluminum. As is shown in Fig. 5c, a 12 µm thick Al foil electrode was indeed found to feature a significantly higher anodic stability in 5.0 M LiFSI dissolved in DMC solution than in 1.0 M LiFSI dissolved in EC:DMC (1:1). Since the

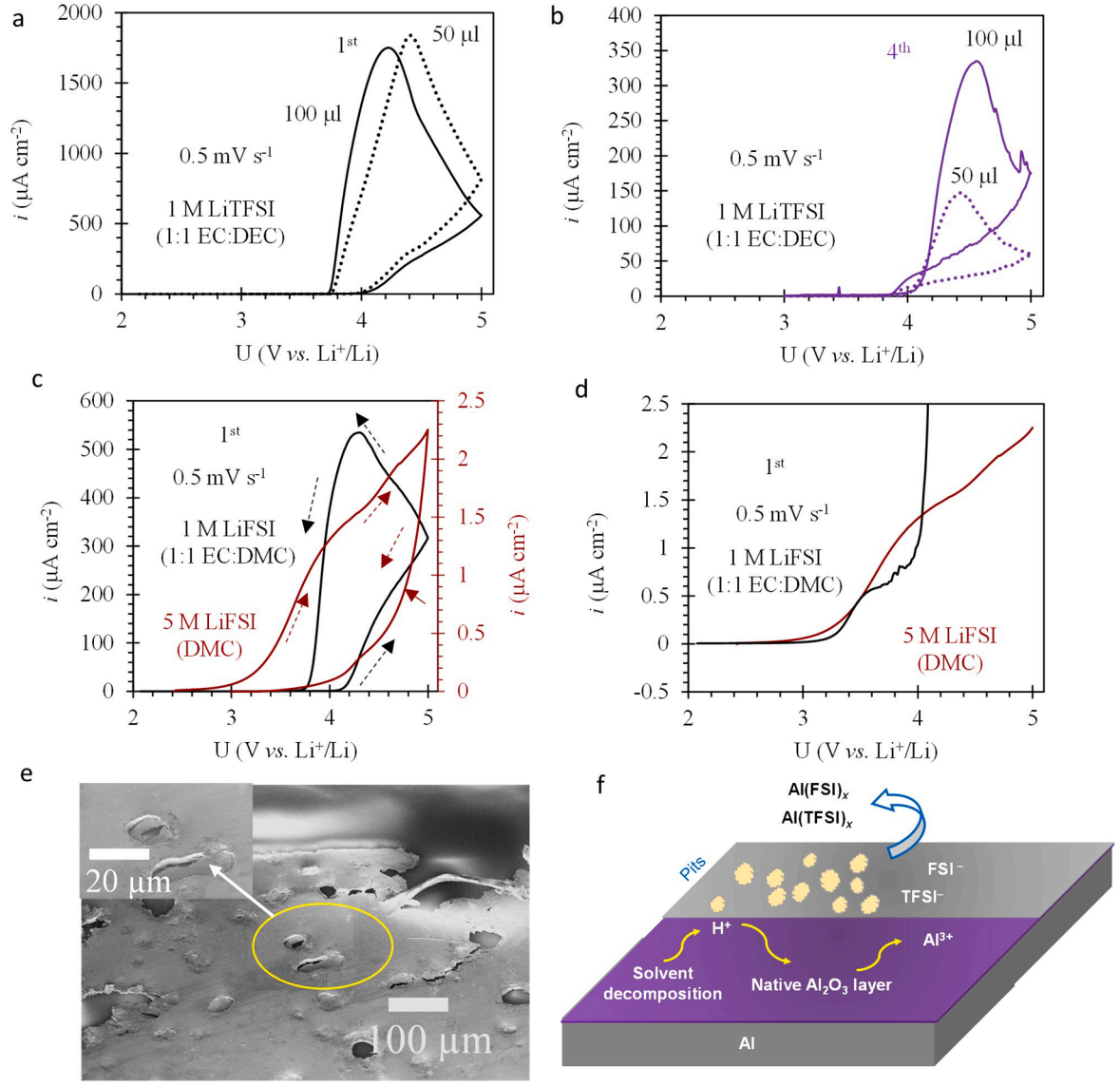

Fig. 5. Effect of the electrolyte volume and salt concentration on the Al anodic dissolution in carbonate electrolytes containing imide salts: (a) and (b) Cyclic voltammograms depicting the first and fourth cycles recorded in 100 µl (solid line) and 50 µl (dotted line) of 1.0 M LiTFSI EC:DEC (1:1), respectively, at a scan rate of 0.5 mV s^{-1}. (c) First cycle voltammograms obtained in 50 µl of 1.0 M LiTFSI EC:DEC (black) and 5.0 M LiFSI DMC (brown), respectively, at a scan rate of 0.5 mV s^{-1}. (d) Linear sweep voltammograms recorded with a 12 µm-thick Al foil electrode in 1.0 M LiTFSI EC:DEC (1:1) (black) and 5.0 M LiFSI DMC (brown), respectively, using a scan rate of 0.5 mV s^{-1}. Note the two oxidation steps. (e) SEM images of the Al foil after cycling in 1.0 M LiTFSI EC:DEC (1:1) electrolyte. The inset shows a high magnification SEM image of the pits. (f) Schematic illustration of the two-step oxidation process occurring in carbonate electrolytes containing LiTFSI or LiFSI.

first cycle anodic current density was only about 2 µA cm^{-2}, the performance seen in the 5.0 M LiFSI electrolyte was in fact very similar to that seen in 1.0 M $LiPF_6$ in Fig. 2a. This similarity also included the presence of a two-step oxidation on the first cycle (see Fig. 5c and d) and the formation of a passive layer on the subsequent cycles. In addition, long-term stability was observed during 300 cycles (see Fig. S3a and b). These findings together with the similar XPS results presented in Fig. 1e indicate that a passive AlF_3 layer was formed also in the 5.0 M LiFSI electrolyte. This is, however, somewhat surprising as an AlF_3 layer only should be expected to form when fluoride (or PF_6^-) is present in the electrolyte. But why would fluoride be present in the 5.0 M electrolyte? This is in fact not that surprising as the manufacturer's specifications indicate that the LiFSI salt may contain up to 100 ppm fluoride as an impurity. This means that the 5.0 M LiFSI electrolyte could have contained a sufficient amount of fluoride to allow the formation of a passive AlF_3 layer, whereas the amount of fluoride most likely was too low in the 1.0 LiFSI electrolyte. This finding is, incidentally, in good agreement with previous reports (Wang et al., 2000) demonstrating that the anodic stability of Al electrodes in LiTFSI or LiFSI based electrolytes can be improved dramatically by the inclusion of sufficiently high concentrations of $LiPF_6$ in the electrolytes. This can be explained by the dissociation of PF_6^- into PF_5 and F^-; (Zhang and Devine, 2006; Stich et al., 2018) allowing a passive AlF_3 layer to be formed. For lower concentrations of LiFSI (e.g., 1.0 M), the concentration of fluoride in the electrolyte may, on the other hand, not be high enough, as indicated by Fig. 4. These findings clearly show that presence of fluoride as an impurity in the electrolytes needs to be considered in conjunction with LiTFSI and LiFSI electrolytes.

2.5. *Effect of a carbon-coating on the performance of Al electrodes in carbonate electrolytes*

In order to decrease the rate of the anodic dissolution of Al in e.g., LiTFSI and LiFSI electrolytes the use of different types of carbon coatings

on Al electrodes have been proposed. (Bizot et al., 2021; Zhang et al., 2020; Li et al., 2019; Prabakar and Pyo, 2012) While good results during a few cycles have been obtained, the long-time stability of the carbon coatings during cycling up to 5.0 V vs. Li^+/Li may, however, still be an issue. According to thermodynamics carbon should be oxidized to CO_2 at potentials above about 3 V vs. Li^+/Li. Long-time cycling experiments were therefore performed in which carbon-coated Al foil electrodes (i.e., 16 μm-thick Al foils with a 1 μm-thick carbon coating) were employed based on their previously reported high anodic stability in imide electrolytes. (Bizot et al., 2021; Zhang et al., 2020; Li et al., 2019; Prabakar and Pyo, 2012) As can be seen in Fig. 6 a, b and c, the first cycle voltammograms for the C-coated Al in 1.0 M $LiPF_6$ EC:DEC (1:1), 1.0 M LiTFSI EC:DEC (1:1), and 5.0 M LiFSI DMC featured oxidation current densities of about 8, 160, 10 and μA cm^{-2}, respectively. After the first scan, passivation was observed in 1.0 M $LiPF_6$ EC:DEC (1:1) and 5.0 M LiFSI DMC but not in the 1.0 M LiTFSI EC:DEC (1:1) electrolyte. In the latter electrolyte, the oxidation current density, however, gradually decreased during the cycling.

A closer look at the 1.0 M $LiPF_6$ EC:DEC (1:1) results shows that the oxidation current density of the C-coated Al was approximately ten times higher than that for the Al foil (i.e., ~ 8 compared to ~ 0.6 μA cm^{-2}), see Fig. 6d. This could be explained by the higher surface area of the C-coated Al (see the SEM images in Figs. S4a and b). Although the oxidation onset potential was slightly higher for the C-coated Al, i.e., about 3.3 compared to about 3.0 V vs. Li^+/Li (see Table 1 and Fig. S4c), a two-step oxidation was still observed with the C-coated Al electrodes (see Fig. S4c). A stable passive behavior was also seen during 300 cycles (see Figs. S4d and e). These results suggest that an AlF_3 passive layer was formed underneath the carbon surface coating. It can hence be concluded that no major difference was seen between the Al and C-coated Al electrodes in the 1.0 M $LiPF_6$ EC:DEC (1:1) case. The larger irreversible first cycle oxidation charge for the C-coated Al (i.e., about 20 mC cm^{-2} compared to ~ 1.9 mC cm^{-2} for the Al foil) should, however, be duly noted.

As shown in Fig. 6e, the maximum first cycle oxidation current density for the C-coated Al in the 1.0 M LiTFSI EC:DEC (1:1) electrolyte was, one the other hand, significantly lower than for the Al foil electrode (i.e., 160 compared to 1800 μA cm^{-2}). This indicates that the carbon coating did decrease the Al anodic dissolution rate in 1.0 M LiTFSI in good agreement with previous reports. (Zhang et al., 2020; Li et al., 2019; Richard Prabakar et al., 2013; Cho et al., 2021) Note also the two-step oxidation with an oxidation onset potential of about 3.6 V vs. Li^+/Li (see Fig. S5a) and the stable behavior during about 200 cycles (see Figs. S5b and c). The magnitude of the first cycle oxidation charge (i.e., about 0.550C/cm^2) and the gradual passivation seen during the first 10 cycles would, however, still constitute a significant problem in practical applications.

Given that the anodic dissolution of aluminum, most likely, is driven by the oxidation of the solvent (thus generating protons which then attack the Al_2O_3 passive layer), it is not surprising that the carbon coating merely could slow down the anodic dissolution somewhat. Based on the similarities between the performances of the Al and C-coated Al electrodes in 1.0 M LiTFSI EC:DEC (1:1) electrolyte, it is also reasonable to assume that the observed gradual passivation was caused by saturation of the electrolyte in the vicinity of the electrode with respect to e.g., $Al(FSI)_x$ species. Since the C-coating would act as a porous layer on top of the Al electrode it is possible that a higher local concentration of the Al species was obtained at the C-coated Al electrode. The diffusion of the generated $Al(FSI)_x$ species into the bulk of the electrolyte would thus be less straightforward with the C-coated Al electrodes. This would explain the lower first cycle oxidation charge and the otherwise analogous passivation process seen with the C-coated Al electrodes. Based on these findings it is immediately clear that the anodic dissolution problem could not be solved using these C-coated Al electrodes. This is, however, not surprising as a proper passive layer could not be attained due to the lack of PF_6^- or F^- ions in the electrolyte.

The results obtained for the C-coated foils in the 5.0 M LiFSI DMC electrolyte (see Fig. 6f) mainly differed from those of the Al electrode in that the first cycle oxidation current density increased significantly at about 4.1 V vs. Li^+/Li and as several reduction peaks could be seen between about 4.4 and 3.7 V vs. Li^+/Li on the subsequent cathodic scan. This indicates that the carbon layer was oxidized and reduced and that

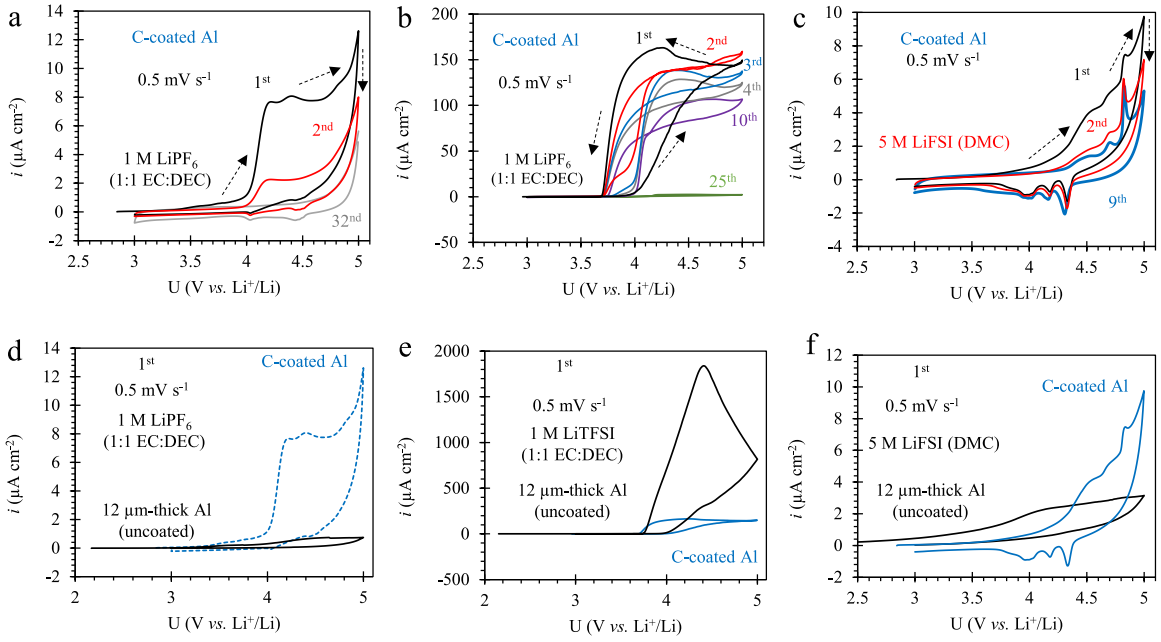

Fig. 6. The electrochemical performances of C-coated Al foil electrodes in some carbonate electrolytes: (a), (b), and (c) Cyclic voltammograms for different cycle numbers recorded in 1.0 M $LiPF_6$ EC:DEC (1:1), 1.0 M LiTFSI EC:DEC (1:1), and 5.0 M LiFSI DMC, respectively, using a scan rate of 0.5 mV s^{-1}. (d), (e), and (f) Comparison of the first cycle voltammograms for a 12 μm-thick Al foil (black) and a C-coated Al (blue) foil electrode in 1.0 M $LiPF_6$ EC:DEC (1:1), 1.0 M LiTFSI EC:DEC (1:1), and 5 M LiFSI DMC, respectively. The scan rate was 0.5 mV s^{-1}. (For interpretation of the references to colour in this figure legend, the reader is referred to the web version of this article.)

this resulted in intercalation and deintercalation of FSI^-, respectively, in agreement with previous findings. (Kotronia et al., 2021) This process did, however, not appear to be reversible as the first cycle oxidation charge was significantly higher than the reduction charge (i.e., 11 compared to 1.2 mC cm^{-2}). The first cycle oxidation charge was, nevertheless, still lower than that obtained in the 1.0 M LiTFSI EC:DEC (1:1) electrolyte, and a robust passive behavior was also seen during 300 cycles (see Fig. S6b). SEM images recorded after the cycling, however, indicated that the cycling had given rise to a partial decomposition of the surface of the carbon coating (see Fig. S6c and d). Since the results for the Al and C-coated Al electrodes were generally very similar, the passivation seen for the C-coated electrode can most likely also be explained by the formation of an AlF_3 passive layer as a result of the presence of fluoride impurities in the electrolyte. The use of the C-coated Al electrodes did consequently not give rise to any additional advantages compared to that of an uncoated Al electrode in the 5.0 M LiFSI DMC electrolyte.

3. Conclusions

The results of this systematic study of the anodic dissolution of Al foils in carbonate-based electrolytes containing $LiPF_6$, LiTFSI or LiFSI at potentials up to 5.0 V vs. Li^+/Li most likely indicate that the anodic dissolution of aluminum is caused by an increase in the concentration of protons at the electrode surface due to the onset of solvent oxidation at about 3 V vs. Li^+/Li. A two-step oxidation process is seen in all electrolytes where the first step involves the oxidation of the carbonate solvents (EC, DEC, DMC, and EMC) whereas the seconds step involves the oxidation of aluminum. This aluminum oxidation step is a consequence of the decrease in the thickness of the Al_2O_3 layer due to its reaction with the protons. In electrolytes containing 1.0 M $LiPF_6$ the degree of anodic dissolution of aluminum is, however, very low as a surface layer of AlF_3 is formed when Al_2O_3 reacts with the formed protons (or HF). This formation of AlF_3 via e.g., the reaction $Al^{3+} + 3HF = AlF_3 + 3H^+$ would be facilitated by the fact that a release of H^+ and Al^{3+} at the electrode surface would shift the equilibrium of the reaction $H^+ + PF_6^- \leftrightarrow PF_5 + HF$ to the right. The experimental results consequently indicate that generation of HF at the electrode surface is needed in order to obtain passivation for Al electrodes in electrolytes containing $LiPF_6$.

In 1.0 M LiFSI and LiTFSI there was, on the other hand, rapid anodic dissolution of aluminum. A corresponding formation of AlF_3 was clearly not possible in these cases due to the absence of PF_6^- in the electrolyte. This is not unexpected as the complexes formed between Al^{3+} and $TFSI^-$ or FSI^- should be more soluble than AlF_3. It is therefore very difficult to use Al electrodes at potentials above 3 V vs. Li^+/Li in electrolytes containing 1.0 M LiFSI or 1.0 M LiTFSI. It was, however, found that the anodic dissolution of aluminum only took place in the potential region in which the solvent(s) most likely were oxidized. This can be explained as follows; when the proton concentration at the electrode surface had decreased sufficiently, the equilibrium of the reaction, $6H^+ + Al_2O_3 \leftrightarrow 3\,H_2O + 2\,Al^{3+}$ was shifted to the left, thus, enabling the generation of a passive Al_2O_3 layer. During repeated cycling in 1.0 M LiFSI or LiTFSI a gradual decrease in the initially very high oxidation current density could also be seen. This effect can be ascribed to a gradual saturation of the electrolytes with respect to the $Al(FSI)_x$ or $Al(TFSI)_x$ species. This type of passivation is, however, of very little practical interest due to the large irreversible capacity associated with this phenomenon.

Passivation, analogous to that seen in 1.0 M $LiPF_6$ was, however, unexpectedly seen in an electrolyte containing 5.0 M LiFSI. The experimental results indicate that this effect most likely stemmed from a formation of an AlF_3 passive layer. This may be explained by the fact that the LiFSI salt may have contained up to 100 ppm of fluoride as an impurity. Care should therefore be taken when interpreting results obtained with highly concentrated LiFSI (or LiTFSI) electrolytes.

The present results likewise indicate that the use of carbon-coated Al electrode is unlikely to solve the Al anodic dissolution problem in electrolytes containing 1.0 M LiTFSI or 1.0 M LiFSI. Although lower Al anodic dissolution rates were found for the carbon coated Al electrodes in 1.0 M LiTFSI, the anodic dissolution rates were still too high to allow practical use of this approach.

As the results obtained with the 12 μm-thick Al foil were analogous to those for the benchmark 20 μm-thick Al foil it is reasonable to assume that the 12 μm-thick Al foil likewise can be used as the current collector for the positive electrode.

The present results show that attempts to find alternatives to $LiPF_6$ when using carbonate solvents should be focused on salts that can give rise to passive layers that are stable in contact with the H^+ produced during the oxidation of the carbonate solvents. This insight may pave the way for high-voltage Li-ion batteries containing conventional carbonate solvents.

4. Experimental

Materials: The 12 μm Al foil was supplied by Gränges Sweden AB, Finspång, Sweden, while the 20 μm Al foil as well as 16 μm-thick carbon-coated Al foil were purchased from MTI. The carbonate electrolytes used in this work and the manufacturers are listed below: 1.0 M $LiPF_6$ EC:DEC (1:1) (Solvionics, H_2O level $<$ 20 ppm), 1.0 M $LiPF_6$ EC:DMC (1:1) (Aldrich, H_2O level $<$ 15 ppm), 1.0 M $LiPF_6$ DEC (Aldrich, H_2O level $<$ 15 ppm), 1.0 M $LiPF_6$ DMC (Aldrich, H_2O level $<$ 15 ppm), 1.2 M $LiPF_6$ EC:EMC (3:7) (Solvionics, H_2O level $<$ 20 ppm), 1.0 M LiFSI EC:DMC (1:1) (Solvionics, H_2O level $<$ 20 ppm), 1.0 M LiTFSI EC:DEC (1:1) (Solvionics, H_2O level $<$ 20 ppm), and 5.0 M LiFSI DMC (Solvionics, H_2O level $<$ 20 ppm).

Materials characterization: The morphology of the Al foil (12-μm-thick) and C-coated foil was characterized using scanning electron microscopy (Zeiss LEO 1550). The cycled cells were transferred to the Ar filled glove box for disassembly, the Al foil was retrieved, washed with DMC, and sealed in Al pouch under vacuum. The sealed Al foil was then transferred directly into the SEM instrument. Prior to the XPS analyses the Al foils were retrieved from the cycled cells inside a glove box and allowed to dry in the glovebox atmosphere. The washed samples were rinsed with a few drops of dimethyl carbonate (DMC). The Al samples were mounted horizontally on a sample holder which were pumped to a low pressure and then transferred without air exposure to the measurement system. The XPS measurements were performed with a Kratos AXIS Supra + X-ray photoelectron spectrometer using a monochromatic Al K_α X-ray source and charge neutralization.

Cell assembly: Pouch cells with Al (for the working electrode) and Cu (for the counter electrode) current collectors were used, were assembled inside an Ar filled glove box (O_2 level $<$ 1 ppm, and H_2O level $<$ 1 ppm). The working electrodes were Al disks with a diameter of 10 mm while lithium metal disks with diameter 13–15 mm diameter were used as combined counter and reference electrodes. The Al working electrodes were dried overnight under vacuum at 120 °C. A piece of dried glass fiber (17 mm diameter, 0.25 mm thickness) soaked in the battery electrolyte (50 μl) was used as the separator. In some experiments 100 μl of the electrolyte was instead used. All measurements were performed using a MPG2 Biologic potentiostat. The cyclic voltammetry experiments were generally conducted in a potential range between 3.0 and 5.0 V (vs. Li^+/Li) at a scan rate 0.5 mV s^{-1}. In the linear sweep voltammetry experiments, the potential was scanned from the open circuit potential (OCP) to 5.0 V at a scan rate 0.5 mV s^{-1}.

Declaration of Competing Interest

The authors declare that they have no known competing financial interests or personal relationships that could have appeared to influence the work reported in this paper.

Data availability

Data will be made available on request.

Acknowledgements

The authors would like to acknowledge financial support from Sweden Battery Center (BASE) and StandUp for Energy. We acknowledge *Myfab* Uppsala for providing facilities and experimental support. *Myfab* is funded by the *Swedish Research Council* as a national research infrastructure.

Appendix A. Supplementary data

Supplementary data to this article can be found online at https://doi.org/10.1016/j.ces.2023.119346.

References

Aktekin, B., Hernández, G., Younesi, R., Brandell, D., Edström, K., 2022. Concentrated LiFSI–Ethylene carbonate electrolytes and their compatibility with High-Capacity and High-Voltage electrodes. ACS Appl Energy Mater. 5, 585–595. https://doi.org/10.1021/acsaem.1c03096.

Armand, M., Axmann, P., Bresser, D., Copley, M., Edström, K., Ekberg, C., Guyomard, D., Lestriez, B., Novák, P., Petranikova, M., Porcher, W., Trabesinger, S., Wohlfahrt-Mehrens, M., Zhang, H., 2020. Lithium-ion batteries – Current state of the art and anticipated developments. Journal of Power Sources 479, 228708. https://doi.org/10.1016/j.jpowsour.2020.228708.

Baer, D.R., Engelhard, M.H., Gaspar, D.J., Lea, A.S., Windisch, C.F., 2002. Use and limitations of electron flood gun control of surface potential during XPS: two non-homogeneous sample types, Surface and interface. Analysis 33, 781–790. https://doi.org/10.1002/sia.1454.

Baer, D.R., Artyushkova, K., Cohen, H., Easton, C.D., Engelhard, M., Gengenbach, T.R., Greczynski, G., Mack, P., Morgan, D.J., Roberts, A., 2020. XPS guide: Charge neutralization and binding energy referencing for insulating samples. Journal of Vacuum Science & Technology A. 38, 031204 https://doi.org/10.1116/6.0000057.

Bizot, C., Blin, M.-A., Guichard, P., Hamon, J., Fernandez, V., Soudan, P., Gaubicher, J., Poizot, P., 2021. Aluminum current collector for high voltage li-ion battery. Part I: A benchmark study with statistical analysis, Electrochem Commun. 126, 107013 https://doi.org/10.1016/j.elecom.2021.107013.

Bizot, C., Blin, M.-A., Guichard, P., Soudan, P., Gaubicher, J., Poizot, P., 2021. Aluminum current collector for high voltage li-ion battery. Part II: Benefit of the en' safe® primed current collector technology. Electrochemistry Communications 126, 107008. https://doi.org/10.1016/j.elecom.2021.107008.

Carlson, T.A., McGuire, G.E., 1972. Study of the x-ray photoelectron spectrum of tungsten—tungsten oxide as a function of thickness of the surface oxide layer. J Electron Spectros Relat Phenomena. 1, 161–168. https://doi.org/10.1016/0368-2048(72)80029-X.

Cho, E., Mun, J., Chae, O.B., Kwon, O.M., Kim, H.-T., Ryu, J.H., Kim, Y.G., Oh, S.M., 2012. Corrosion/passivation of aluminum current collector in bis(fluorosulfonyl) imide-based ionic liquid for lithium-ion batteries. Electrochemistry Communications 22, 1–3. https://doi.org/10.1016/j.elecom.2012.05.018.

Cho, E., Chang-jian, C.-W., Wu, Y., Chao, S., Huang, J., Lee, K.-C., Weng, H.C., Hsu, S.-C., 2021. Modification of aluminum current collectors with laser-scribed graphene for enhancing the performance of lithium ion batteries. Journal of Power Sources 506, 230060. https://doi.org/10.1016/j.jpowsour.2021.230060.

Gabryelczyk, A., Ivanov, S., Bund, A., Lota, G., 2021. Corrosion of aluminium current collector in lithium-ion batteries: A review. J Energy Storage. 43, 103226 https://doi.org/10.1016/j.est.2021.103226.

Gao, H., Ma, T., Duong, T., Wang, L., He, X., Lyubinetsky, I., Feng, Z., Maglia, F., Lamp, P., Amine, K., Chen, Z., 2018. Protecting al foils for high-voltage lithium-ion chemistries, mater today. Energy 7, 18–26. https://doi.org/10.1016/j.mtener.2017.12.001.

Guo, L., Thornton, D.B., Koronfel, M.A., Stephens, I.E.L., Ryan, M.P., 2021. Degradation in lithium ion battery current collectors. Journal of Physics: Energy. 3, 032015 https://doi.org/10.1088/2515-7655/ac0c04.

Kawamura, T., Tanaka, T., Egashira, M., Watanabe, I., Okada, S., Yamaki, J.I., 2005. Methyl difluoroacetate inhibits corrosion of aluminum cathode current collector for lithium ion cells. Electrochemical and Solid-State Letters. 8 https://doi.org/10.1149/1.1993367.

Kerner, M., Plylahan, N., Scheers, J., Johansson, P., 2016. Thermal stability and decomposition of lithium bis(fluorosulfonyl)imide (LiFSI) salts. RSC Advances 6, 23327–23334. https://doi.org/10.1039/c5ra25048j.

Kerry, J., 2012. Aluminium foil packaging, Packaging. Technology 163–177. https://doi.org/10.1533/9780857095701.2.163.

Kim, J.W., Seong, M.J., Park, D.W., Jeong, G., Yim, T., 2022. Anti-corrosive and surface-stabilizing functional electrolyte containing LiFSI and LiPO2F2 for SiO /NCM811-based batteries. Corrosion Science 198, 110117. https://doi.org/10.1016/j.corsci.2022.110117.

Kotronia, A., Asfaw, H.D., Tai, C.W., Hahlin, M., Brandell, D., Edström, K., 2021. Nature of the Cathode-Electrolyte interface in highly concentrated electrolytes used in graphite Dual-Ion batteries. ACS Applied Materials & Interfaces 13, 3867–3880. https://doi.org/10.1021/acsami.0c18586.

Kramer, E., Passerini, S., Winter, M., 2012. Dependency of aluminum collector corrosion in lithium ion batteries on the electrolyte solvent. ECS Electrochemistry Letters. 1, 9–12. https://doi.org/10.1149/2.004205eel.

Krämer, E., Schedlbauer, T., Hoffmann, B., Terborg, L., Nowak, S., Gores, H.J., Passerini, S., Winter, M., 2013. Mechanism of anodic dissolution of the aluminum current collector in 1 M LiTFSI EC:DEC 3:7 in rechargeable lithium batteries. Journal of the Electrochemical Society 160, A356–A360. https://doi.org/10.1149/2.081302jes.

Li, X., Deng, S., Banis, M.N., Doyle-Davis, K., Zhang, D., Zhang, T., Yang, J., Divigalpitiya, R., Brandys, F., Li, R., Sun, X., 2019. Suppressing corrosion of aluminum foils via highly conductive graphene-like carbon coating in High-Performance Lithium-Based batteries. ACS Applied Materials & Interfaces 11, 32826–32832. https://doi.org/10.1021/acsami.9b06442.

Li, Y., Zhang, X., Khan, S.A., Fedkiw, P.S., 2004. Attenuation of aluminum current collector corrosion in LiTFSI electrolytes using fumed silica nanoparticles. Electrochemical and Solid-State Letters. 7, A228. https://doi.org/10.1149/1.1756857.

Lindgren, F., Rehnlund, D., Källquist, I., Nyholm, L., Edström, K., Hahlin, M., Maibach, J., 2017. Breaking down a complex system: Interpreting PES peak positions for cycled Li-Ion battery electrodes. The Journal of Physical Chemistry C. 121, 27303–27312. https://doi.org/10.1021/acs.jpcc.7b08923.

Ma, T., Xu, G.L., Li, Y., Wang, L., He, X., Zheng, J., Liu, J., Engelhard, M.H., Zapol, P., Curtiss, L.A., Jorne, J., Amine, K., Chen, Z., 2017. Revisiting the corrosion of the aluminum current collector in Lithium-Ion batteries. Journal of Physical Chemistry Letters. 8, 1072–1077. https://doi.org/10.1021/acs.jpclett.6b02933.

Markovsky, B., Amalraj, F., Gottlieb, H.E., Gofer, Y., Martha, S.K., Aurbach, D., 2010. On the electrochemical behavior of aluminum electrodes in nonaqueous electrolyte solutions of lithium salts. Journal of the Electrochemical Society 157, A423–A429. https://doi.org/10.1149/1.3294774.

Matsumoto, K., Inoue, K., Nakahara, K., Yuge, R., Noguchi, T., Utsugi, K., 2013. Suppression of aluminum corrosion by using high concentration LiTFSI electrolyte. Journal of Power Sources 231, 234–238. https://doi.org/10.1016/j.jpowsour.2012.12.028.

Meister, P., Qi, X., Kloepsch, R., Krämer, E., Streipert, B., Winter, M., Placke, T., 2017. Anodic behavior of the aluminum current collector in Imide-Based electrolytes: influence of solvent, operating temperature, and native Oxide-Layer thickness. ChemSusChem 10, 804–814. https://doi.org/10.1002/cssc.201601636.

Metzger, M., Walke, P., Solchenbach, S., Salitra, G., Aurbach, D., Gasteiger, H.A., 2020. Evaluating the High-Voltage stability of conductive carbon and ethylene carbonate with various lithium salts. Journal of the Electrochemical Society 167, 160522. https://doi.org/10.1149/1945-7111/abcabd.

Morita, M., Shibata, T., Yoshimoto, N., Ishikawa, M., 2003. Anodic behavior of aluminum current collector in LiTFSI solutions with different solvent compositions. Journal of Power Sources 119–121, 784–788. https://doi.org/10.1016/S0378-7753(03)00253-2.

Murmann, P., Schmitz, R., Nowak, S., Gores, H., Ignatiev, N., Sartori, P., Passerini, S., Winter, M., Schmitz, R.W., 2013. Electrochemical and thermal investigations and Al current collector dissolution studies of three Di-Lithium salts in comparison to LiPF 6 containing electrolytes. Journal of the Electrochemical Society 160, A535–A541. https://doi.org/10.1149/2.013304jes.

Myung, S.T., Sasaki, Y., Sakurada, S., Sun, Y.K., Yashiro, H., 2009. Electrochemical behavior of current collectors for lithium batteries in non-aqueous alkyl carbonate solution and surface analysis by ToF-SIMS. Electrochimica Acta 55, 288–297. https://doi.org/10.1016/j.electacta.2009.08.051.

Myung, S.T., Hitoshi, Y., Sun, Y.K., 2011. Electrochemical behavior and passivation of current collectors in lithium-ion batteries. Journal of Materials Chemistry 21, 9891–9911. https://doi.org/10.1039/c0jm04353b.

Pender, J.P., Jha, G., Youn, D.H., Ziegler, J.M., Andoni, I., Choi, E.J., Heller, A., Dunn, B. S., Weiss, P.S., Penner, R.M., Mullins, C.B., 2020. Electrode degradation in Lithium-Ion batteries. ACS Nano 14, 1243–1295. https://doi.org/10.1021/acsnano.9b04365.

Piao, N., Wang, L., He, X., 2021. Anodic stabilities of various metals as the current collector in high concentration electrolytes for lithium batteries. Journal of the Electrochemical Society 168, 030509. https://doi.org/10.1149/1945-7111/abe8ba.

Prabakar, S.J.R., Pyo, M., 2012. Corrosion protection of aluminum in LiPF 6 by poly (3, 4-ethylenedioxythiophene) nanosphere-coated multiwalled carbon nanotube. Corrosion Science 57, 42–48. https://doi.org/10.1016/j.corsci.2011.12.036.

Richard Prabakar, S.J., Hwang, Y., Bae, E.G., Lee, D.K., Pyo, M., 2013. Graphene oxide as a corrosion inhibitor for the aluminum current collector in lithium ion batteries. Carbon N Y. 52, 128–136. https://doi.org/10.1016/j.carbon.2012.09.013.

Solchenbach, S., Metzger, M., Egawa, M., Beyer, H., Gasteiger, H.A., 2018. Quantification of PF 5 and POF 3 from side reactions of LiPF 6 in Li-Ion batteries. Journal of the Electrochemical Society 165, A3022–A3028. https://doi.org/10.1149/2.0481813jes.

Stich, M., Göttlinger, M., Kurniawan, M., Schmidt, U., Bund, A., 2018. Hydrolysis of LiPF6 in Carbonate-Based electrolytes for Lithium-Ion batteries and in aqueous media. Journal of Physical Chemistry C. 122, 8836–8842. https://doi.org/10.1021/acs.jpcc.8b02080.

Strohmeier, B.R., 1990. An ESCA method for determining the oxide thickness on aluminum alloys, surface and interface. Analysis 15, 51–56. https://doi.org/10.1002/sia.740150109.

Wang, X., Yasukawa, E., Mori, S., 2000. inhibition of anodic corrosion of aluminum cathode current collector on recharging in lithium imide electrolytes. Electrochimica Acta 45, 2677–2684. https://doi.org/10.1016/S0013-4686(99)00429-6.

Whitehead, A.H., Schreiber, M., 2005. Current collectors for positive electrodes of Lithium-Based batteries. Journal of the Electrochemical Society 152, A2105. https://doi.org/10.1149/1.2039587.

Wu, X., Du, Z., 2021. Study of the corrosion behavior of LiFSI based electrolyte for li-ion cells. Electrochemistry Communications 129, 107088. https://doi.org/10.1016/j.elecom.2021.107088.

Yamada, Y., Chiang, C.H., Sodeyama, K., Wang, J., Tateyama, Y., Yamada, A., 2015. Corrosion prevention mechanism of aluminum metal in superconcentrated electrolytes. ChemElectroChem 2, 1687–1694. https://doi.org/10.1002/celc.201500235.

Yoon, E., Lee, J., Byun, S., Kim, D., Yoon, T., 2022. Passivation failure of al current collector in LiPF 6 -Based electrolytes for Lithium-Ion batteries. Advanced Functional Materials 32, 2200026. https://doi.org/10.1002/adfm.202200026.

Zhang, X., Devine, T.M., 2006. Identity of passive film formed on aluminum in Li-Ion battery electrolytes with LiPF6. Journal of the Electrochemical Society 153, B344. https://doi.org/10.1149/1.2214465.

Zhang, X., Devine, T.M., 2006. Factors that influence formation of AlF[sub 3] passive film on aluminum in Li-Ion battery electrolytes with LiPF[sub 6]. Journal of the Electrochemical Society 153, B375. https://doi.org/10.1149/1.2218816.

Zhang, S.S., Jow, T.R., 2002. Aluminum corrosion in electrolyte of li-ion battery. Journal of Power Sources 109, 458–464. https://doi.org/10.1016/S0378-7753(02)00110-6.

Zhang, G., Lin, K., Qin, X., Zhang, L., Li, T., Lv, F., Xia, Y., Han, W., Kang, F., Li, B., 2020. Electrosprayed robust graphene layer constructing ultrastable electrode interface for High-Voltage Lithium-Ion batteries. ACS Applied Materials & Interfaces 12, 37034–37046. https://doi.org/10.1021/acsami.0c06698.

Zhang, X., Winget, B., Doeff, M., Evans, J.W., Devine, T.M., 2005. Corrosion of aluminum current collectors in Lithium-Ion batteries with electrolytes containing LiPF[sub 6]. Journal of the Electrochemical Society 152, B448. https://doi.org/10.1149/1.2041867.

Zhang, S.S., Xu, K., Jow, T.R., 2002. Study of LiBF[sub 4] as an electrolyte salt for a Li-Ion battery. Journal of the Electrochemical Society 149, A586. https://doi.org/10.1149/1.1466857.

Zhu, P., Gastol, D., Marshall, J., Sommerville, R., Goodship, V., Kendrick, E., 2021. A review of current collectors for lithium-ion batteries. Journal of Power Sources 485, 229321. https://doi.org/10.1016/j.jpowsour.2020.229321.